Transmission through a biased graphene bilayer barrier

Johan Nilsson,[1] A. H. Castro Neto,[1] F. Guinea,[2] and N. M. R. Peres[3]

[1]*Department of Physics, Boston University, 590 Commonwealth Avenue, Boston, Massachusetts 02215, USA*
[2]*Instituto de Ciencia de Materiales de Madrid, CSIC, Cantoblanco, E28049 Madrid, Spain*
[3]*Center of Physics and Departamento de Física, Universidade do Minho, P-4710-057 Braga, Portugal*

We study the electronic transmission through a graphene bilayer in the presence of an applied bias between the layers. We consider different geometries involving interfaces between both a monolayer and a bilayer and between two bilayers. The applied bias opens a sizable gap in the spectrum inside the bilayer barrier region, thus leading to large changes in the transmission probability and electronic conductance that are controlled by the applied bias.

I. INTRODUCTION

The idea of carbon based electronics has been around since the discovery of carbon nanotubes almost 15 years ago. Much progress has been made but many problems associated with manufacturability remain still to be resolved (see, for example, the recent reviews in Refs. 1 and 2). Recently, another possible platform for carbon based electronics was discovered in graphene,[3] i.e., a two-dimensional (2D) honeycomb lattice of carbon atoms that can be viewed either as a single layer of graphite or an unrolled nanotube. The electric field effect has already been demonstrated in these systems: by tuning a gate bias voltage, one can control both the type (electrons or holes) and the number of carriers.[4,5] For a recent review on the rise of graphene, see Ref. 6.

One fundamental difficulty with most of the graphene devices studied so far is the experimental fact that there exists a universal (sample independent) maximum in the resistivity of the order of 6.5 kΩ near the Dirac point in all these systems.[4] This relatively small resistivity limits the performance of devices via a poor on-off ratio. The reason for the nonzero minimal conductivity is the peculiar gapless spectrum and presence of disorder in the samples. Several theoretical studies using different methods find a universal minimum in the conductivity in some limits. However, the reason for it and its exact value varies[7–14] (see also the recent review in Ref. 15). There has also been a number of earlier theoretical studies of junctions and barriers in both monolayer and bilayer graphene systems.[9,13,16–19]

One way of getting around the minimal conductivity is to use nanoribbons made out of graphene. Because of the confinement, these systems are generally found to be gapped,[20] which is consistent with recent experiments.[21] In this paper, we propose another simple geometry that transforms the semimetallic graphene into a semiconductor with a truly gapped spectrum without confinement. The presence of a gap makes the properties of the system more robust to perturbations. This is crucial for device performance and possible device integration since imperfections are always present. The basic idea is to use a bilayer region as a barrier for the electrons. By manipulating the electrostatics with gates and/or chemical doping, a gap can appear in the spectrum. By tuning the chemical potential, one can move the system

from sitting inside the gap, where the electronic transmission is exponentially suppressed, into the allowed band regions where the transmission is close to 1. Other interesting features of the proposed geometry are that the gap size can be tuned with gates, allowing for an external control of the electronic properties, and the bilayer can be integrated as one of the components of a pure graphene based device.[22] Recently, barriers made out of double-gated bilayer graphene have been fabricated and characterized in Ref. 23, and their results are consistent with a gate-tunable gap.

The paper is organized as follows. In Sec. II, we introduce the model of the system that we are considering and give explicit expressions for the wave functions. In Sec. III, we match wave functions considering different geometries. In particular, we study a monolayer-bilayer interface, a bilayer-bilayer interface, and two bilayer barrier setups. In the barrier setups, we use either monolayer graphene or bilayer graphene in the leads. In Sec. IV, we present results for the conductance in the different barrier setups. A brief summary and the conclusions of the paper can be found in Sec. V. For completeness, we also provide some details about the self-consistent determination of the gap in Appendix A. In Appendix B, we provide some details of how we compute the transmission amplitudes.

II. MODEL

A schematic picture of the system is shown in Fig. 1. The basic structure involves a graphene sheet extending to the left and to the right of a region where there is a second
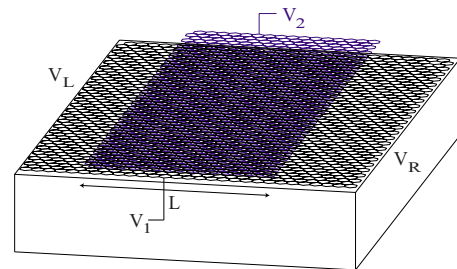

FIG. 1. (Color online) Geometry of the biased graphene bilayer barrier with monolayer leads.

graphene sheet sitting on top of the first, this region is the *bilayer barrier* (BB) region. The whole structure is assumed to sit on top of a dielectric spacer insulating the graphene from a back gate. Later on (Sec. III E), we will also consider a system where the regions to the left and right of the barrier are made out of graphene bilayers. We will refer to the two systems as having monolayer and bilayer leads.

To the left (L) and to the right (R) of the barrier, the low-energy effective Hamiltonian (near the K point of the Brillouin zone) has the form of the 2D Dirac Hamiltonian,[24]

$$\mathcal{H}_\alpha = v_F \begin{pmatrix} V_\alpha/v_F & k_x + ik_y \\ k_x - ik_y & V_\alpha/v_F \end{pmatrix}, \quad (1)$$

where $\mathbf{k}=(k_x,k_y)$ is the 2D momentum measured relative to the K point, $\alpha=L,R$, and $v_F \approx 10^6$ m/s is the Fermi-Dirac velocity (we use units such that $\hbar=1=v_F$ from now on). The Dirac Hamiltonian acts on a spinor representing the wave functions on the two sublattices: $\psi=(\psi_{A1},\psi_{B1})^T$. In the following, we mostly work with the case where $V_L=V_R=0$ so that the energy is measured with respect to the Dirac point in the monolayer regions. The spectrum of the Hamiltonian in Eq. (1) is then simply $E_\pm(k)=\pm k$ ($k^2=k_x^2+k_y^2$), where the plus (minus) sign is associated with electron (hole) states. The low-energy effective bilayer Hamiltonian has the form (see, e.g., Refs. 25 and 26)

$$\mathcal{H}_{BB} = \begin{pmatrix} V_1 & q_x+iq_y & t_\perp & 0 \\ q_x-iq_y & V_1 & 0 & 0 \\ t_\perp & 0 & V_2 & q_x-iq_y \\ 0 & 0 & q_x+iq_y & V_2 \end{pmatrix}. \quad (2)$$

Here, the two-dimensional momentum is $\mathbf{q}=(q_x,q_y)$ and the corresponding spinor is $\psi=(\psi_{A1},\psi_{B1},\psi_{A2},\psi_{B2})^T$. $t_\perp \approx 0.35$ eV is the hopping energy between nearest neighbor atoms in different planes (i.e., A1 and A2). The monolayer is connected to plane 1 in the bilayer. Solving for the spectrum of the Hamiltonian in Eq. (2), one finds four energy bands given by

$$E_{\pm,s}(q) = (V_1 + V_2)/2$$
$$\pm \sqrt{q^2 + \frac{V^2}{4} + \frac{t_\perp^2}{2} + s\frac{1}{2}\sqrt{4(V^2+t_\perp^2)q^2+t_\perp^4}}, \quad (3)$$

where $s=\pm$ and $V=V_1-V_2$. Thus, for the two bands closest to the Dirac point ($E_{\pm,-}$), the spectrum is gapped and has an unusual "Mexican hat" dispersion, as was pointed out in Ref. 25. There exists other examples in the literature of materials with a similar dispersion, often called "camel-back" dispersion instead of Mexican hat. This feature can arise—like in our case—in the $\mathbf{k}\cdot\mathbf{p}$ approximation when two bands that are close to each other in energy are allowed to hybridize. Examples of materials where a camel-back has been proposed include tellurium,[27] GaP,[28] and GaAs.[29]

The *crucial property* for the structure proposed here is that we allow for different voltages on the two layers in the BB region: $V_1 \neq V_2$. This possibility have been noted before,[25,30] but here we are exploiting this feature. These potentials can be created by a uniform electric field through

the bilayer that generates a charge imbalance between the two layers. In a transport measurement, the graphene is connected to electron reservoirs and can hence become charged. When voltages are applied to the gates and the graphene structure, charge is redistributed to minimize the total electrostatic energy. The problem is basically that of a capacitor. Upon studying the problem, the bilayer must be viewed as a single unit since the planes are connected by orbital overlap. For example, the induced charge imbalance between the layers will screen the applied electric field; $t_\perp$ also works against the applied field since it tends to equalize the densities in the two planes.

A simple estimate of these effects is provided by a self-consistent Hartree theory (see Appendix A and Refs. 26 and 31). For an isolated uncharged infinite bilayer, we find that the net effect is to replace the applied voltage difference V by a smaller effective V_{MF}. For some reasonable parameters [$V<t_\perp$ and interlayer distance $d\approx 3.35-3.6$ Å (Refs. 32 and 33)], V_{MF} is down by a factor of order 3 compared with the bare value. In particular, for an experimentally accessible voltage drop of 90 V over 300 nm, we find an effective voltage difference of $V_{MF} \sim 40$ meV. This value might be improved upon incorporating a dielectric (e.g., SiO_2) and/or using a thinner dielectric spacer. Thus, it is not unreasonable to have $V_{MF} \sim 100$ meV. This estimate was done before we became aware of the measurements reported in Refs. 34 and 35. In the first of these references, the gap is measured in angle-resolved photoelectron spectroscopy to be as large as 200 meV, but the charge densities are also quite large in their case [$n \sim (1-6) \times 10^{13}$ cm^{-2}]. In the second reference, the maximum obtained gap is estimated to be ~ 100 meV. The largest possible value of the gap is estimated to be ~ 300 meV and is limited by the dielectric breakdown of the SiO_2.

Experimentally, the bias can be controlled by different methods. The conceptually simplest and most flexible method is to use a back gate and a top gate (like in a dual gate metal-oxide-semiconductor field-effect transistor geometry), preferably using split gates and therefore allowing for different gate voltages in the monolayer and bilayer regions. It is worth to mention that local top gates have already been successfully fabricated on single-layer graphene samples.[36–39] The field is progressing rapidly since, for example, only a year ago, no top gate had been reported in graphene systems. Moreover, very recently, a top gate was also fabricated on bilayer graphene and characteristics consistent with a gate-tunable gap were reported.[23] Another possibility is to change the chemical environment by depositing donor or acceptor molecules on top of the structure.[34,35] These act like dopants in a semiconductor and allow for independent control of the bias and the chemical potential. Note, however, that this method always introduces impurities into the system with potentially important consequences.[40]

On symmetry grounds, a more general Hamiltonian than the one in Eq. (2) is certainly allowed, as discussed in Ref. 41 for the case of graphite. For example, the couplings γ_3 and γ_4 associated with electron hopping between carbon atoms that are not nearest neighbors in different layers, familiar to the graphite literature, are possible.[32] In the BB, the effects of these terms are less important than for the low-

energy features in graphite since the gap is a robust feature in the low-energy spectrum of the BB. The electrostatic response in different sublattices within each layer is also likely to be different, that is, one should use $V_{A1} \neq V_{B1}$, etc. If the applied voltage difference is not too large compared with $t_\perp$, the implications of this effect are presumably small. The applied field and the pressure from anything on the top of the structure will probably affect both the interlayer distance and the interlayer coupling. The details of the band structure including all the effects above is a very complicated problem that has yet to be studied. Nevertheless, we believe that the Hamiltonian in Eq. (2) correctly captures the main features of the spectrum, including the important formation of the gap in the spectrum near the Dirac point. In view of the large uncertainty in the parameters involved, it is meaningless to pursue a more complicated model at this point. The inclusion of the other parameters introduces no principal problems, but the analysis becomes more complicated.

A. Eigenvectors

The normalized energy E eigenvectors of $\mathcal{H}_\alpha$ in Eq. (1) can be written as

$$\bar{v}_\alpha = \frac{1}{\sqrt{2(E-V_\alpha)}} \begin{pmatrix} E - V_\alpha \\ k_x - ik_y \end{pmatrix}, \tag{4}$$

when the particles are "on shell,"

$$(E - V_\alpha)^2 = k_x^2 + k_y^2. \tag{5}$$

A simple way to generate the eigenvectors of $\mathcal{H}_{BB}$ in Eq. (2) is to note that the columns of the Green's function G^0 in the bilayer region ($G^0 = [E - \mathcal{H}_{BB}]^{-1}$) are proportional to the eigenvectors if the relation between the energy E and the momentum **q** are on shell. It is straightforward albeit tedious to generalize this approach to the more general Hamiltonians discussed above. Using this, we extract two different energy E eigenvectors of $\mathcal{H}_{BB}$ as

$$\bar{v}_{BB,A1} = \begin{pmatrix} [(E-V_2)^2 - q_x^2 - q_y^2](E-V_1) \\ [(E-V_2)^2 - q_x^2 - q_y^2](q_x - iq_y) \\ t_\perp(E-V_2)(E-V_1) \\ t_\perp(E-V_1)(q_x + iq_y) \end{pmatrix} \tag{6}$$

and

$$\bar{v}_{BB,A2} = \begin{pmatrix} t_\perp(E-V_2)(E-V_1) \\ t_\perp(E-V_2)(q_x - iq_y) \\ [(E-V_1)^2 - q_x^2 - q_y^2](E-V_2) \\ [(E-V_1)^2 - q_x^2 - q_y^2](q_x + iq_y) \end{pmatrix}. \tag{7}$$

These just differ by their overall normalization. It is straightforward to check that these vectors are indeed eigenvectors of $\mathcal{H}_{BB}$ in Eq. (2) by direct substitution. The on-shell condition in the bilayer region reads

$$2(q_x^2 + q_y^2) = (E - V_1)^2 + (E - V_2)^2 \pm \sqrt{[(E-V_1)^2 - (E-V_2)^2]^2 + 4t_\perp^2(E-V_1)(E-V_2)}. \tag{8}$$

III. DIFFERENT GEOMETRIES

In this section, we compute the transmission amplitudes for different edges and geometries. By convention, the incident wave is taken to arrive from the left side of the barrier and is transmitted to the right.

A. Zigzag termination with monolayer leads

With our conventions, the zigzag termination of the barrier corresponds to cutting the strip along the y direction. For simplicity, we consider the case that the width W of the structure is large enough so that the boundary conditions in the transverse direction are irrelevant. It is then convenient to assume periodic boundary conditions and use translational invariance and fix $k_y = q_y$ to be a good quantum number in addition to the energy E. This assumption can be relaxed.[9,19,42] When the width becomes small enough that the quantization of the transverse momentum becomes important, the system becomes similar to a semiconducting nanotube with a finite radius. As discussed by Brey and Fertig, it is a good approximation to use the continuum description of a graphene ribbon if it is wide enough and provided that the proper boundary conditions for the continuous model are

employed.[43] For the zigzag edges, one can work in the single valley approximation and the correct boundary condition is to take the wave function to vanish in one of the sublattices (A2 on the left and B2 on the right in our case) at the BB boundaries. We choose the energy E and $k_y = |E|\sin(\phi)$ so that there are propagating states to the left of the junction, with $k_x = E\cos(\phi)$. The four solutions of Eq. (8) for q_x inside the bilayer are denoted by $\pm q_{x1}$ and $\pm q_{x2}$.

B. Monolayer-bilayer interface

Consider the step geometry where there is no right end of the bilayer. Then, one must only keep states that propagate to the right or decay as one moves into the bilayer. Thus, to the left, we take the wave function to be

$$\bar{\psi}_L = 1\bar{v}_{L,+}e^{ik_x x} + r\bar{v}_{L,-}e^{-ik_x x}, \tag{9}$$

where r is the reflection amplitude and $\bar{v}_{L\pm}$ are the spinors associated with the sublattices given in Eq. (4). In the bilayer, one has
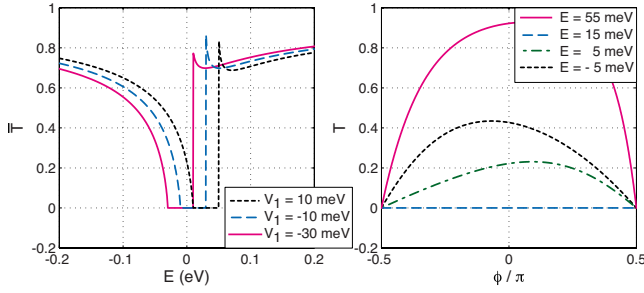
FIG. 2. (Color online) Transmission amplitudes in the monolayer-bilayer step geometry. Left: energy dependence of $\bar{T}$ for $V_2-V_1=40$ meV and different values of V_1. Right: angular dependence of $T(E,\phi)$ for $V_1=10$ meV and $V_2=50$ meV and different values of the energy.

$$\bar{\psi}_{BB} = a_{1+}\bar{v}_{BB,1+}e^{iq_{x1}x} + a_{2+}\bar{v}_{BB,2+}e^{iq_{x2}x}, \qquad (10)$$

where $a_{1(2)\pm}$ are scattering amplitudes and $\bar{v}_{BB,1(2)\pm}$ the respective spinors computed from Eq. (6) or (7). Matching of the wave functions only involves their continuity. Because the associated differential equation is of first order, this is sufficient to ensure current conservation. Explicitly, the boundary conditions are

$$\bar{\psi}_L(x=0)\big|_{A1} = \bar{\psi}_{BB}(x=0)\big|_{A1}, \qquad (11a)$$

$$\bar{\psi}_L(x=0)\big|_{B1} = \bar{\psi}_{BB}(x=0)\big|_{B1}, \qquad (11b)$$

$$\bar{\psi}_{BB}(x=0)\big|_{A2} = 0. \qquad (11c)$$

From this, we compute (for details, see Appendix B) the transmission probability $T(E,\phi)=1-|r|^2$ and the angular averaged transmission probability

$$\bar{T}(E) = \int_{-\pi/2}^{\pi/2} \frac{d\phi}{\pi} T(E,\phi). \qquad (12)$$

Some representative results are shown in Fig. 2. There are two features that are apparent in the figure. (a) There is a small asymmetry between the angles $\pm\phi$. Hence, a current of electrons without valley polarization leads to a transmitted current with a finite valley polarization. This is not the case at other boundaries, like a potential step applied to a graphene monolayer or a graphene bilayer.[17] The breaking of the symmetry between the two Dirac points arises from the lack of time reversal symmetry, as we consider a current carrying state, and the lack of inversion symmetry, induced by the zigzag bilayer edge or the bias potential in the bilayer (for a general discussion, see Ref. 44, and for a particular discussion, see Appendix B). As a result, the barrier discussed here can be used as a device which creates a valley polarized current.[45] (b) There is a clear asymmetry between positive and negative energies. This can be understood by noting that the monolayer is coupled to layer 1 in the bilayer. When the energy is tuned to V_1, the weight on sublattice A1 goes to zero [cf. Eq. (7)]. Consequently, the current in plane 1 is zero at that energy, and hence no current can flow into

the bilayer. It appears as though the current goes continuously to zero as the band edge is approached. At the other edge ($E \sim V_2$) of the band gap, the current in plane 2 is zero [cf. Eq. (6)], but the current can now flow in through the other plane. This fact is responsible for the sharp edge in the transmission amplitude at the conduction band edge.

It is important to choose the momenta for right movers in Eqs. (9) and (10) such that their group velocity $v_g=dE/dq_x$ >0. Otherwise, one may erroneously conclude that $T<0$ for some values of the energy, this is sometimes referred to as the Klein paradox.[46] It is also worth noting that the actual charge distribution near the edge is a complicated problem that involves a self-consistent solution of the Poisson equation and the band structure, beyond the scope of this study. This may lead to corrections to the simple wave function matching we use here. Furthermore, it is known that edges can lead to interesting effects in graphene systems such as edge states and self-doping.[7]

C. Biased bilayer barrier with monolayer leads

Consider the barrier geometry of Fig. 1. We assume the length L of the bilayer region to be large compared to the lattice spacing so that the continuum model is applicable. In this geometry, one also needs the wave function to the right of the barrier,

$$\bar{\psi}_R = t\bar{v}_{R,+}e^{ik_x(x-L)}, \qquad (13)$$

where t is now the transmission amplitude. Inside the barrier, one generally needs all momentum components,

$$\bar{\psi}_{BB} = a_{1+}\bar{v}_{BB,1+}e^{iq_{x1}x} + a_{2+}\bar{v}_{BB,2+}e^{iq_{x2}x} + a_{1-}\bar{v}_{BB,1-}e^{-iq_{x1}x}$$
$$+ a_{2-}\bar{v}_{BB,2-}e^{-iq_{x2}x}. \qquad (14)$$

In this case, in addition to the boundary conditions in Eq. (11), there are also those at the right edge,

$$\bar{\psi}_R(x=L)\big|_{A1} = \bar{\psi}_{BB}(x=L)\big|_{A1}, \qquad (15a)$$

$$\bar{\psi}_R(x=L)\big|_{B1} = \bar{\psi}_{BB}(x=L)\big|_{B1}, \qquad (15b)$$

$$\bar{\psi}_{BB}(x=L)\big|_{B2} = 0. \qquad (15c)$$

It is a simple task to match the boundary conditions and, in this case, one finds six equations for the six unknowns: t, r, a_{1+}, a_{1-}, a_{2+}, and a_{2-}. The results for $T(E,L,\phi)=|t|^2$ for some representative parameters are shown in Fig. 3. The oscillations in the transmission amplitudes are due to the possibility of having resonances inside the BB region. For example, in the right panel of Fig. 3, the two energies are chosen such that they have the same q^2 computed from Eq. (8) for the propagating mode. In one case ($E=5$ meV), $|E|\sin(\phi)=q_y \ll q$ and the resonances are pronounced with the distance between consecutive maxima approximately given by $\pi/q_x \sim \pi/q \sim 25$ nm. In the other case ($E=-45$ meV), $|E|\sin(\phi)=q_y \sim q$ and most of the resonance phenomena averages out upon performing the angle average because of the larger variation of q_x.
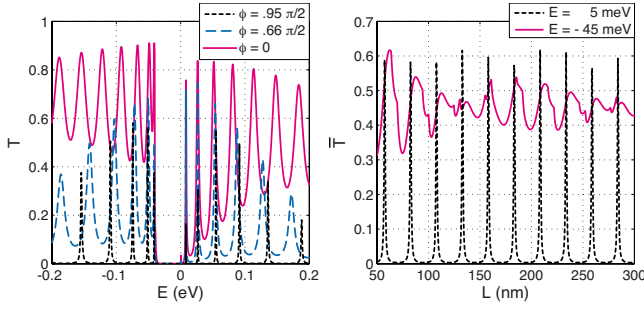
FIG. 3. (Color online) Transmission amplitudes in the BB with monolayer leads. Left: energy dependence of $T(E, L, \phi)$ for different angles and $L = 50$ nm. Right: length dependence of $\overline{T}(E, L)$ for different energies. In both the figures, $V_1 = 0$ and $V_2 = -40$ meV.

D. Armchair termination

The calculations for the armchair geometry is similar albeit more involved since one cannot work in the single cone approximation.[43] In this case, one must instead mix the valleys to be able to fulfill the boundary conditions so that the wave functions on both of the lattice sites in layer 2 vanish at the boundaries. This doubles the size of the matrix problem that must be solved. For example, to compute the transmission amplitudes in the BB geometry, one must solve a system of 12 equations. The calculation is a straightforward extension of the case above and although the shapes of the curves are not exactly the same, there are no new features except for a parity effect associated with the number of unit cells in the barrier. This is related to the modulo 3 effect found in the spectrum of an armchair graphene nanoribbon in the nearest neighbor tight-binding approximation.[43]

E. Bilayer-bilayer step and biased bilayer barrier with bilayer leads

It is important to note that it is not necessary to have the BB region defined by actually cutting the second graphene sheet. Another possibility is to use a bilayer throughout and to use a local top gate to create a local gap and hence a barrier in the bilayer. As we shall see, the characteristics of this type of junction are better than the one with the monolayer leads. In particular, the oscillations in the transmission amplitudes and conductivities are much smaller because the matching between two bilayers is usually better than between a monolayer and a bilayer.

We will consider the simple case that the bilayer in the L and R regions is essentially gapless; we also assume that $|E| < t_\perp$ for the incoming wave as this will likely be the experimental situation. Since the gapless bilayer is a special case of the gapped bilayer with no gap, we may use the formulas and spinors from Sec. II A directly with $V_1 = V_2 = 0$. This case was considered in Ref. 13 and allows for some further simplifications of the spinors, but that is not necessary here.

The incoming wave is taken to be a traveling wave with absolute momentum given by $k^2 = |E|(t_\perp + |E|)$. As in the above, we define $k_x = \pm k \cos(\phi)$ and $k_y = k \sin(\phi)$. One should
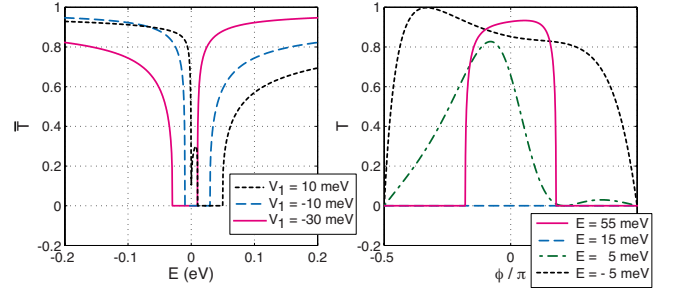

FIG. 4. (Color online) Transmission amplitudes in the unbiased bilayer–biased bilayer step geometry. Left: energy dependence of $\overline{T}$ for $V_2 - V_1 = 40$ meV and different values of V_1. Right: angular dependence of $T(E, \phi)$ for $V_1 = 10$ meV and $V_2 = 50$ meV and different values of the energy.

also take care to define the sign of k_x for the incoming wave so that the wave is a right mover. We will denote the corresponding spinors by $\overline{v}_{B0,\alpha}$, where $\alpha = \pm$ goes with $\exp(\pm i k_x x)$ and denotes right and left movers, respectively. To be able to fulfill the boundary conditions, one must also consider the decaying modes,[17] which will have an imaginary value of the momentum in the x direction: $k_x = i \kappa_x$. One can show that the correct value is $\kappa_x = \sqrt{|E|(t_\perp - |E|) + k_y^2}$. We write as $\overline{v}_{B0,i\alpha}$ in an obvious notation the corresponding spinors.

The calculation proceeds exactly as in the other cases when one has identified the particular incoming propagating mode in the bilayer to the left,

$$\overline{\psi}_L = 1 \overline{v}_{B0,+} e^{ik_x x} + r \overline{v}_{B0,-} e^{-ik_x x} + r' \overline{v}_{B0,-i} e^{\kappa_x x}. \quad (16)$$

Now, we can consider a step geometry where the incoming wave from the unbiased bilayer propagates into a biased bilayer. In this case, the spinor in Eq. (16) should be matched with the one in Eq. (10) at $x = 0$. More details for this case are provided in Appendix B. Some representative results are shown in Fig. 4, and these should be contrasted with the case of a monolayer-bilayer step in Fig. 2. Note that the asymmetry between $\pm \phi$ is also present in this case. For the case of a bilayer barrier with bilayer leads, the spinor to the right is

$$\overline{\psi}_R = t \overline{v}_{B0,+} e^{ik_x(x-L)} + t' \overline{v}_{B0,i} e^{-\kappa_x(x-L)}. \quad (17)$$

The wave functions in Eqs. (16) and (17) should be matched with the one in Eq. (14) to the left and to the right. In this case, the correct boundary conditions are to take all of the components of the 4-spinor wave function to be continuous at the two boundaries of the BB region. The transmission amplitude is in this case given by $T(E, \phi) = |t|^2$. An example of the transmission amplitudes is shown in Fig. 5. It is clear that the magnitudes of the oscillations in the amplitudes are much smaller than in the cases involving monolayer leads. Moreover, the pronounced resonances found in the length dependence of Fig. 3 is largely gone in this case. This is probably due to the fact that the wave functions of two bilayers are better matched than those of a monolayer and a bilayer. It is also interesting to note that the effective gap becomes larger than the actual gap in the BB for larger values of the angles. This is due to the fact that, given the
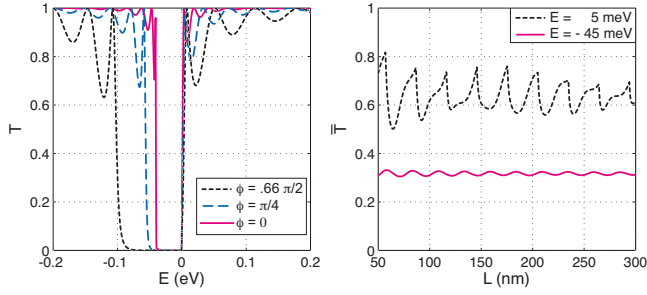
FIG. 5. (Color online) Transmission amplitudes in the BB with bilayer leads. Left: energy dependence of $T(E,L,\phi)$ for different angles and $L=50$ nm. Right: length dependence of $\bar{T}(E,L)$ for different energies. In both the figures, $V_1=0$ and $V_2=-40$ meV.

energy, the absolute value of the momentum is much larger in the bilayer than the monolayer. Consequently, one has to go to larger values of the energy in Eq. (8) to have a mode that is not decaying inside the BB region.

IV. RESULTS FOR THE CONDUCTANCE

Using the Landauer formula (see, e.g., Ref. 47), we find that the current across the BB is given by

$$I = \frac{2e}{h} \int dE \sum_n |t_n(E)|^2 [f(E-\mu_R) - f(E-\mu_L)]. \quad (18)$$

Here, f is the Fermi distribution function and μ_L (μ_R) is the chemical potential in the left (right) lead. n labels the modes and $t_n(E)$ the corresponding transmission amplitude at energy E. From this, the finite temperature linear response conductance can be computed as a function of the overall chemical potential μ,

$$G(\mu) = -\frac{4e^2}{h} \int dE M(E)\bar{T}(E)\frac{\partial f(E-\mu)}{\partial E}. \quad (19)$$

For the BB with monolayer leads, $M(E) \sim W|E|/\pi$ is the number of transverse propagating modes in the monolayer at energy E. For bilayer leads, the relation is instead $M(E) \sim W\sqrt{|E|(t_\perp+|E|)}/\pi$. At zero temperature, the expression in Eq. (19) simplifies to
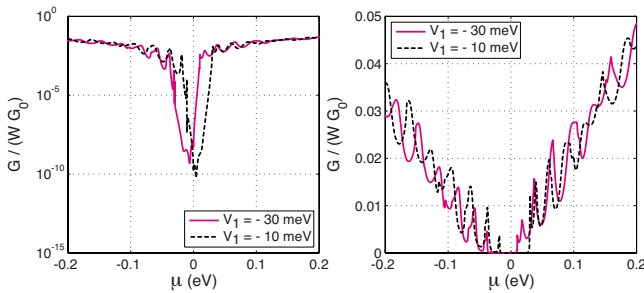

FIG. 6. (Color online) Left (right): semilogarithmic (linear) plot of the zero-temperature conductance divided by the width W (in nm) of the BB device with monolayer leads in units of $G_0=4e^2/h$ as a function of the chemical potential μ. $V_2-V_1=40$ meV and $L=50$ nm.
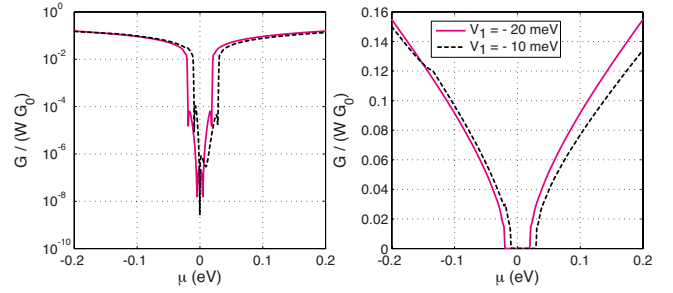

FIG. 7. (Color online) Left (right): semilogarithmic (linear) plot of the zero-temperature conductance divided by the width W (in nm) of the BB device with bilayer leads in units of $G_0=4e^2/h$ as a function of the chemical potential μ. $V_2-V_1=40$ meV and $L=50$ nm.

$$G(\mu) = \frac{4e^2}{h}M(\mu)\bar{T}(\mu). \quad (20)$$

Some results are presented in Figs. 6 and 7. As expected, if the barrier is wide enough and the energy is tuned to be inside the gap, the conductance is strongly suppressed. Outside of this region, the conductance is larger by many orders of magnitude. It is also clear from Eq. (19) that a finite temperature T will lead to a smearing of any sharp feature on an energy scale of approximately $4T$. Nevertheless, as long as the temperature is much smaller than the gap, large on-off ratios are possible.

Let us finally comment on possible effects associated with roughness or impurities at the edges of the sample. These will induce some intervalley scattering and lead to an angle average. This may be a serious problem for the proposals which emphasize the angular dependence of the transmission.[17] Because we are considering the transmission integrated over the angles, this should only weakly affect our results. The resonances are also likely to survive in a real sample when many incoming modes overlap with one of the eigenmodes of the BB region. Roughness at the ends of the BB will probably broaden the resonances, however.

V. SUMMARY AND CONCLUSIONS

We have studied the problem of electronic transmission through a graphene bilayer barrier as a function of applied voltage between the layers and the overall chemical potential. We have considered two types of devices, one with monolayer leads and one with bilayer leads. In the first type, the barrier region is defined by having a bilayer only in a small part of the sample. In the second type of device, the barrier is instead defined by a local gate in a system made entirely out of a graphene bilayer. The latter system seems to have a smoother electronic characteristic due to the absence of sharp boundaries that are present in the first device. We have shown that the transmission probability and the electronic conductance are strongly dependent on the applied bias, leading to the possibility of applying this geometry for carbon based electronics.

APPENDIX A: SELF-CONSISTENT DETERMINATION OF THE GAP

It is important to note that due to the polarization of the BB, the actual size of the potential difference V between the planes is not equal to the bare externally applied potential difference V_0. A simple approximation that takes into account the screening of the external field by the BB is to include the interaction among the electrons within the BB at the Hartree level in a self-consistent manner. Such a calculation was applied for the half-filled case for the preprint of the present paper, and it was worked out independently at the same time for a more general case by McCann in Ref. 26. More recent works along these lines include a joint experimental-theory paper[35] and *ab initio* calculations.[31] There has also been a study of the screening of an external electric field in graphene multilayer systems in the *A-B* stacking.[48]

In this appendix, we provide details of the self-consistent determination of the gap. In particular, we give explicit analytic expressions for all of the quantities involved in the nonlinear equation that needs to be solved. These expressions are potentially useful for anyone who wish to apply this simple theory.

1. Hartree approximation

Charges on the two planes in the bilayer lead to an electrostatic energy given by the capacitive coupling

$$E_c = -2\pi de^2 S n_1 n_2, \tag{A1}$$

in the simplest approximation of two uniformly charged planes. First, we decouple the contributions from the total density $n = n_1 + n_2$ and the density difference $\delta n = n_2 - n_1$. Here, we are interested in the latter term, which we will treat in the Hartree mean field approximation. Denoting by $\langle \delta n(V_{MF}) \rangle$ the expectation values of δn in the ground state of the mean field Hamiltonian [i.e., Eq. (2) with the substitution $V_1 - V_2 = V \rightarrow V_{MF}$], the mean field equation can be written as

$$V_{MF} = V_0 - 2\pi de^2 \langle \delta n(V_{MF}) \rangle, \tag{A2}$$

where the expressions for $\langle \delta n \rangle$ at half-filling is given below in Eq. (A3). If all the energies are expressed in eV, the mean field equations becomes simply $V_{MF} \approx V_0 - 7.3 \langle \delta n(V_{MF}) \rangle$. The solution of the mean field equations at half-filling, is shown in Fig. 8. Away from half-filling, one must also include the corrections due to the partial filling of the conduction or valence band.
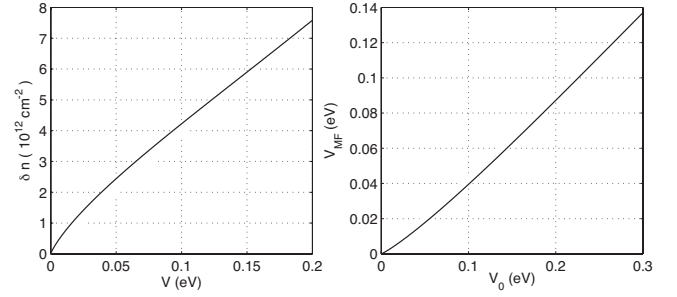

FIG. 8. Left: occupation asymmetry δn at half-filling as a function of the bias V. Right: self-consistently determined value of the bias potential V_{MF} as a function of the applied potential V_0.

An important quantity for the self-consistent determination of the gap size is the density difference between the layers δn. In the simple model we are using, this quantity depends on $t_\perp$, V, and the density n. At half-filling, when the chemical potential is sitting inside the gap, the result to leading order in the cutoff (see below) is

$$\delta n = \frac{V}{2\pi(t_\perp^2 + V^2)^{3/2}} \left\{ V\sqrt{t_\perp^2 + V^2}[(V^2/2 + t_\perp^2) + V\sqrt{t_\perp^2 + V^2/4}] + t_\perp^2(t_\perp^2 + V^2/2)\ln\left[\frac{t_\perp^2 + V^2/2 + \sqrt{t_\perp^2 + V^2/4}\sqrt{t_\perp^2 + V^2}}{(\sqrt{t_\perp^2 + V^2} - V)V/2} \right] \right\}. \tag{A3}$$

The occupation asymmetry δn as a function of V at half-filling is also depicted in Fig. 8. One can easily check that the expression in Eq. (A3) reduces to the correct expression in the limit of decoupled planes ($t_\perp = 0$).

2. Occupation asymmetry at half-filling

First, we introduce the shorthand $N_{\alpha j}/D \equiv G^0_{\alpha j \alpha j}$ for the diagonal components of the bare Green's function that is defined by $G^0 = [\omega - \mathcal{H}_{BB}]^{-1}$. We take $D = \text{Det}[\omega - \mathcal{H}_{BB}]$ and $N_{\alpha j}$ to be the appropriate cofactor of the matrix $[\omega - \mathcal{H}_{BB}]$. Using this, the density of states on sublattice αj can be written as

$$\rho_{\alpha j}(\omega) = \frac{1}{S} \sum_{\beta = \pm} \sum_{\beta' = \pm} \sum_{\mathbf{k}, \sigma} \frac{N_{\alpha j}}{D'(E_{\beta, \beta'})} \delta(\omega - E_{\beta, \beta'}). \tag{A4}$$

Here, the β sums are over the different bands and we have suppressed the frequency and momentum dependences of the functions for brevity. If we want to compute the density difference between the layers $\delta n = n_2 - n_1$ when the chemical potential is sitting inside the gap, we must calculate

$$\delta n = \int_{-\infty}^{0} d\omega [\rho_{A2} + \rho_{B2} - \rho_{A1} - \rho_{B1}]$$

$$= 4 \sum_{\beta = \pm} \int_{0}^{\Lambda} \frac{d^2 \mathbf{k}}{(2\pi)^2} \frac{N_{A2} + N_{B2} - N_{A1} - N_{B1}}{D'(\omega)} \bigg|_{\omega = E_{-,\beta}},$$

$$(A5)$$

which include both spin polarizations and the two valleys. Now, one may use that

$$N_{A2} + N_{B2} - N_{A1} - N_{B1} = -2V(\omega^2 + k^2 - V^2/4 - t_{\perp}^2/2)$$

$$(A6)$$

and

$$D'(E_{\pm,\beta}) = \beta 2 E_{\pm,\beta} \sqrt{4(V^2 + t_{\perp}^2)k^2 + t_{\perp}^4},$$

$$(A7)$$

to write

$$\delta n = \frac{V}{\pi} \int_{0}^{\Lambda^2} \frac{d(k^2)}{\sqrt{4(V^2 + t_{\perp}^2)k^2 + t_{\perp}^4}} \frac{E_{+,+} - E_{+,-}}{E_{+,+}E_{+,-}} [E_{+,+}E_{+,-} - k^2$$

$$+ V^2/4 + t_{\perp}^2/2].$$

$$(A8)$$

Using $E_{+,+}E_{+,-} = \sqrt{(k^2 - V/2)^2 + V^2 t_{\perp}^2/4}$, one can convince oneself that the integral in Eq. (A8) is convergent as $\Lambda \to \infty$ so that the leading term is independent of the cutoff. Changing the integration variable to z defined by

$$z = \sqrt{4(V^2 + t_{\perp}^2)k^2 + t_{\perp}^4},$$

$$(A9)$$

the integral can be performed analytically with the result shown in Eq. (A3).

APPENDIX B: EXPLICIT MATRIX EQUATIONS

In this appendix, we show how to obtain the matrix equations that we then solve numerically to obtain the transmission amplitudes. For the simplest case of a monolayer-bilayer step, using Eqs. (9), (10), (4), and (6), the boundary conditions in Eq. (11) can be rewritten as a matrix equation,

$$\begin{pmatrix} E \\ k_x - ik_y \\ 0 \end{pmatrix} = \begin{pmatrix} E & [(E-V_2)^2 - q_{x1}^2 - k_y^2](E-V_1) & [(E-V_2)^2 - q_{x2}^2 - k_y^2](E-V_1) \\ -k_x - ik_y & [(E-V_2)^2 - q_{x1}^2 - k_y^2](q_{x1} - ik_y) & [(E-V_2)^2 - q_{x2}^2 - k_y^2](q_{x2} - ik_y) \\ 0 & t_{\perp}(E-V_2)(E-V_1) & t_{\perp}(E-V_2)(E-V_1) \end{pmatrix} \begin{pmatrix} -r \\ a_{1+} \\ a_{2+} \end{pmatrix}.$$

$$(B1)$$

For this simple case, it is also possible to work out an explicit expression for r,

$$r = -\frac{E^3 - 2V_2 E^2 - [k_y^2 + q_{x1}^2 + q_{x2}^2 - V_2^2 + q_{x1}q_{x2} - k_x(q_{x1} + q_{x2})]E - (k_x - ik_y)(q_{x1} + q_{x2})V_1}{E^3 - 2V_2 E^2 - [k_y^2 + q_{x1}^2 + q_{x2}^2 - V_2^2 + q_{x1}q_{x2} + k_x(q_{x1} + q_{x2})]E + (k_x + ik_y)(q_{x1} + q_{x2})V_1}.$$

$$(B2)$$

Now, one can substitute the correct values of the momenta [cf. Eq. (8)] such that the incoming state is a right mover and that only states that decay or propagate to the right inside the bilayer are present. We note that for energies such that q_{x1} is real and q_{x2} is imaginary—which is often the case for energies such that $V \lesssim |E - (V_1 + V_2)/2| \lesssim t_{\perp}$—the transformation $k_y \to -k_y$ is in general not simply associated with a phase of r. Consequently, there is an asymmetry in the transmission amplitude, as shown in Fig. 2.

The reason for the asymmetry is the broken inversion symmetry. Either the symmetry is broken by a zigzag edge of the bilayer or by the bias field. It is clear that the bias potential breaks the inversion symmetry in the point in the middle between the two A atoms of the unit cell. This is crucial as it breaks the sublattice symmetry that is otherwise present. It is also important that there exists a mode that is evanescent as this breaks the symmetry between states with k_y and $-k_y$ when one is matching the wave functions. For if all momenta

are real, one can easily convince oneself that to solve for $-k_y$ one must only take the complex conjugate of the solution with k_y; thus, the only difference is the phase between r and r^*, which will not affect the transmission amplitude. In addition, it is necessary that there exists a mode that can transmit the current. Otherwise, all of the incoming current is reflected and no asymmetry can be generated; note that this is the case for a monolayer with a gap.

The other more complicated cases involves 6×6 and 8×8 matrices. The procedure to obtain the transmission amplitude is a straightforward generalization of the example worked out above, but the full forms of the matrices are too long to write out here. The matrix inversion is then performed numerically.

Another interesting example is to match a wave coming in from an unbiased bilayer and propagating into a biased bilayer. In this case, the matrix equation can be written as

$$
\begin{pmatrix}
-E \\
-(k_x - ik_y) \\
|E| \\
\mathrm{sgn}(E)(k_x + ik_y)
\end{pmatrix}
$$

$$
=
\begin{pmatrix}
-E & E & [(E-V_2)^2 - q_{x1}^2 - k_y^2](E-V_1) & [(E-V_2)^2 - q_{x2}^2 - k_y^2](E-V_1) \\
-(-k_x - ik_y) & (-i\kappa_x - ik_y) & [(E-V_2)^2 - q_{x1}^2 - k_y^2](q_{x1} - ik_y) & [(E-V_2)^2 - q_{x2}^2 - k_y^2](q_{x2} - ik_y) \\
|E| & |E| & t_\perp (E-V_1)(E-V_2) & t_\perp (E-V_1)(E-V_2) \\
\mathrm{sgn}(E)(-k_x + ik_y) & \mathrm{sgn}(E)(-i\kappa_x + ik_y) & t_\perp (E-V_1)(q_{x1} + ik_y) & t_\perp (E-V_1)(q_{x2} + ik_y)
\end{pmatrix}
\begin{pmatrix}
-r \\
-r' \\
a_{1+} \\
a_{2+}
\end{pmatrix}.
$$

$$(B3)$$

Here, we have used the fact that the spinors simplify in the leads where the inversion symmetry is not broken (i.e., $V_1 = V_2 = 0$).[13] Also in this case, one finds that there is an asymmetry between negative and positive angles within each valley. In this case, this is due to the fact that the inversion symmetry is broken by the bias potential in the BGB. In the case of $V_1 = V_2 \neq 0$, the inversion symmetry is not broken and the transmission is symmetric between $\pm k_y$.[17]

---

[1] P. L. McEuen, M. S. Fuhrer, and H. Park, IEEE Trans. Nanotechnol. **1**, 78 (2002).

[2] P. Avouris, J. Appenzeller, R. Martel, and S. J. Wind, Proc. IEEE **91**, 1772 (2003).

[3] K. S. Novoselov, A. K. Geim, S. V. Morozov, D. Jiang, Y. Zhang, S. V. Dubonos, I. V. Gregorieva, and A. A. Firsov, Science **306**, 666 (2004).

[4] K. S. Novoselov, A. K. Geim, S. V. Morozov, D. Jiang, M. I. Katsnelson, I. V. Grigorieva, S. V. Dubonos, and A. A. Firsov, Nature (London) **438**, 197 (2005).

[5] Y. Zhang, Y.-W. Tan, H. L. Stormer, and P. Kim, Nature (London) **438**, 201 (2005).

[6] A. K. Geim and K. S. Novoselov, Nat. Mater. **6**, 1476 (2007).

[7] N. M. R. Peres, F. Guinea, and A. H. Castro Neto, Phys. Rev. B **73**, 125411 (2006).

[8] M. I. Katsnelson, Eur. Phys. J. B **51**, 157 (2006).

[9] J. Tworzydlo, B. Trauzettel, M. Titov, A. Rycerz, and C. W. J. Beenakker, Phys. Rev. Lett. **96**, 246802 (2006).

[10] J. Nilsson, A. H. Castro Neto, F. Guinea, and N. M. R. Peres, Phys. Rev. Lett. **97**, 266801 (2006).

[11] M. I. Katsnelson, Eur. Phys. J. B **52**, 151 (2006).

[12] K. Nomura and A. H. MacDonald, Phys. Rev. Lett. **98**, 076602 (2007).

[13] I. Snyman and C. W. J. Beenakker, Phys. Rev. B **75**, 045322 (2007).

[14] J. Cserti, Phys. Rev. B **75**, 033405 (2007).

[15] A. H. Castro Neto, F. Guinea, N. M. R. Peres, K. S. Novoselov, and A. K. Geim, arXiv:0709.1163v1 (unpublished).

[16] V. V. Cheianov and V. I. Fal'ko, Phys. Rev. B **74**, 041403(R) (2006).

[17] M. I. Katsnelson, K. S. Novoselov, and A. K. Geim, Nat. Phys. **2**, 620 (2006).

[18] J. M. Pereira, V. Mlinar, F. M. Peeters, and P. Vasilopoulos, Phys. Rev. B **74**, 045424 (2006).

[19] P. G. Silvestrov and K. B. Efetov, Phys. Rev. Lett. **98**, 016802 (2007).

[20] Y.-W. Son, M. L. Cohen, and S. G. Louie, Phys. Rev. Lett. **97**, 216803 (2006).

[21] M. Y. Han, B. Ozyilmaz, Y. Zhang, and P. Kim, Phys. Rev. Lett. **98**, 206805 (2007).

[22] C. Berger *et al.*, J. Phys. Chem. B **108**, 19912 (2004).

[23] J. B. Oostinga, H. B. Heersche, X. Liu, A. F. Morpurgo, and L. M. K. Vandersypen, arXiv:0707.2487v1 (unpublished).

[24] P. R. Wallace, Phys. Rev. **71**, 622 (1947).

[25] F. Guinea, A. H. Castro Neto, and N. M. R. Peres, Phys. Rev. B **73**, 245426 (2006).

[26] E. McCann, Phys. Rev. B **74**, 161403(R) (2006).

[27] M. von Ortenberg and K. J. Button, Phys. Rev. B **16**, 2618 (1977).

[28] R. G. Humphreys, U. Rössler, and M. Cardona, Phys. Rev. B **18**, 5590 (1978).

[29] H. Im, L. E. Bremme, P. C. Klipstein, A. V. Kornilov, H. Beere, D. Ritchie, R. Grey, and G. Hill, Phys. Rev. B **70**, 205313 (2004).

[30] E. McCann and V. I. Fal'ko, Phys. Rev. Lett. **96**, 086805 (2006).

[31] H. Min, B. Sahu, S. K. Banerjee, and A. H. MacDonald, Phys. Rev. B **75**, 155115 (2007).

[32] N. B. Brandt, S. M. Chudinov, and Y. G. Ponomarev, *Semimetals 1: Graphite and its Compounds* (North-Holland, Amsterdam, 1988).

[33] S. D. Chakarova-Kack, E. Schroder, B. I. Lundqvist, and D. C. Langreth, Phys. Rev. Lett. **96**, 146107 (2006).

[34] T. Ohta, A. Bostwick, T. Seyller, K. Horn, and E. Rotenberg, Science **313**, 951 (2006).

[35] E. V. Castro, K. S. Novoselov, S. V. Morozov, N. M. R. Peres, J. M. B. Lopes dos Santos, J. Nilsson, F. Guinea, A. K. Geim, and A. H. Castro Neto, arXiv:cond-mat/0611342v1 (unpublished).

[36] M. Lemme, T. Echtermeyer, M. Baus, and H. Kurz, IEEE Electron Device Lett. **28** (2007).

[37] B. Huard, J. A. Sulpizio, N. Stander, K. Todd, B. Yang, and D. Goldhaber-Gordon, Phys. Rev. Lett. **98**, 236803 (2007).

[38] B. Özyilmaz, P. Jarillo-Herrero, D. Efetov, D. A. Abanin, L. S. Levitov, and P. Kim, arXiv:0705.3044v2 (unpublished).

[39] J. R. Williams, L. DiCarlo, and C. M. Marcus, Science **317**, 638 (2007).

[40] J. Nilsson and A. H. Castro Neto, Phys. Rev. Lett. **98**, 126801

(2007).

[41] J. C. Slonczewski and P. R. Weiss, Phys. Rev. **109**, 272 (1958).

[42] N. M. R. Peres, A. H. Castro Neto, and F. Guinea, Phys. Rev. B **73**, 195411 (2006).

[43] L. Brey and H. A. Fertig, Phys. Rev. B **73**, 235411 (2006).

[44] J. L. Mañes, F. Guinea, and M. A. H. Vozmediano, Phys. Rev. B **75**, 155424 (2007).

[45] A. Rycerz, J. Tworzydlo, and C. W. J. Beenakker, Nat. Phys. **3**, 172 (2007).

[46] A. Calogeracos and N. Dombey, Contemp. Phys. **40**, 313 (1999).

[47] S. Datta, *Electronic Transport in Mesoscopic Systems* (Cambridge University Press, Cambridge, 1995).

[48] F. Guinea, Phys. Rev. B **75**, 235433 (2007).